JOURNAL OF MATERIALS SCIENCE **38** (2003) 853–864

Crystallization study of (TiO_2,ZrO_2)-rich SiO_2-Al_2O_3-CaO glasses

Part II *Surface and internal crystallization processes investigated by differential thermal analysis (DTA)*

P. LOISEAU, D. CAURANT*, O. MAJERUS, N. BAFFIER
Laboratoire de Chimie Appliquée de l'Etat Solide (UMR CNRS 7574), ENSCP, 11 rue Pierre et Marie Curie, 75231 Paris, France
E-mail: caurant@ext.jussieu.fr

C. FILLET
Commissariat à l'énergie atomique (CEA), Direction de l'Energie Nucléaire, Centre de la Vallée du Rhône, DIEC/SCDV/LEBM, 30207 Bagnols sur Ceze, France

Controlled crystallization of (TiO_2-ZrO_2)-rich calcium aluminosilicate glasses led to zirconolite in the bulk, and titanite and anorthite on the surface. Such glass-ceramics can be envisaged for minor actinides immobilization. In this study, the crystallization of three glass compositions with increasing TiO_2, ZrO_2 and CaO amounts was followed by differential thermal analysis (DTA). The effect of glass particle size and of heating rate on DTA curves was studied in order to investigate nucleation mechanisms and to extract the corresponding crystal growth activation energies E_c for the different crystalline phases. Exothermic effects associated with the crystallization of a phase having a defect-fluorite structure in the bulk and its consecutive transformation into zirconolite were only detected for the highly TiO_2, ZrO_2 and CaO enriched glasses due to their higher crystallization rate. Using an Avrami constant $n = 3$ and a dimensionality of crystal growth $m = 3$, the activation energy of defect-fluorite crystal growth was found to be $E_c = 440$ kJ · mol^{-1} (modified Kissinger method). Titanite and anorthite grow only from glass surface with activation energies of respectively 493 and 405 kJ · mol^{-1} ($n = m = 1$, Kissinger method). DTA study of melt crystallization during cooling showed that baddeleyite (ZrO_2) crystals firstly crystallize but become unstable versus zirconolite for higher undercooling.

1. Introduction

Investigations are currently performed in different countries on new matrices for the specific immobilization of long-lived radionuclides such as minor actinides (Np, Am and Cm) that would originate from an enhanced reprocessing of nuclear spent fuel. Similar studies are also in progress for excess weapons plutonium waste immobilization. Glass-ceramics containing highly durable crystals accommodating large amounts of actinides, such as zirconolite (nominally $CaZrTi_2O_7$) [1–3], are good candidates for this application.

In part I of this work [4], it was showed that appropriate (TiO_2-ZrO_2)-rich calcium aluminosilicate glass compositions led to zirconolite crystallization in the bulk of the glass after isothermal treatment (nucleation + crystal growth) whereas a thin layer mainly composed of titanite and anorthite crystals formed on samples surface. A strong effect of parent glass composition—and particularly of TiO_2 and ZrO_2 amounts—on the zirconolite nucleation rate and on the total amount of crystals was observed. Nd^{3+} ions—selected as trivalent minor actinides surrogate—partition between residual glass and zirconolite crystals in the bulk of glass-ceramics; in zirconolite crystals, Nd^{3+} ions mainly substitute for Ca^{2+} ions. For the glass-ceramics exhibiting the highest proportion of crystalline phase, approximately 43% of the total amount of neodymium is incorporated in the zirconolite phase.

In this paper, crystallization of the three glass compositions reported in [4] was followed by differential thermal analysis (DTA). The effect of glass particle size and heating rate on exothermic peaks was studied in order to investigate nucleation mechanisms and to extract the crystal growth activation energies for the phases formed on the surface and in the bulk of the glass. The

*Author to whom all correspondence should be addressed.

TABLE I Composition (in oxide weight and molar percentage) and glass transformation temperature of glasses A, B and C

	SiO_2	Al_2O_3	CaO	TiO_2	ZrO_2	Nd_2O_3	Na_2O	T_g (°C)
Glass A								
weight%	40.57	11.95	19.63	12.45	8.46	6.00	0.94	762 ± 2
mol%	48.23	8.37	25.01	11.14	4.90	1.27	1.08	
Glass B								
weight%	36.07	10.62	19.18	15.98	11.31	6.00	0.84	760 ± 2
mol%	43.83	7.61	24.97	14.61	6.70	1.30	0.98	
Glass C								
weight%	32.47	9.56	18.82	18.81	13.59	6.00	0.75	760 ± 2
mol%	40.17	6.97	24.94	17.50	8.20	1.32	0.90	

results are compared with the X-ray diffraction (XRD) and the scanning electron microscopy (SEM) results reported in [4]. The behavior of the melt during cooling was also studied.

2. Experimental

Compositions of the three glasses A, B and C studied in this work are given in Table I. They correspond to progressively TiO_2-ZrO_2 enriched SiO_2-Al_2O_3-CaO glasses. A constant 6 weight% Nd_2O_3 amount was used to simulate nuclear waste for all the samples. The glass preparation method and the problems encountered during melting of the compositions B and C were described in Part I of this work [4].

DTA was used in order to study glass devitrification processes and other irreversible transformations which occurred during heating (exothermic effects), crystals dissolution in the residual glass (endothermic effects) and melt crystallization during cooling (exothermic effects). This technique was also used to determine the glass transition temperature (onset of the endothermic effect). The DTA measurements were performed between 300 and 1250–1650°C under air with a NETZSCH STA 409 thermal analysis apparatus. Between 100 and 200 mg of as quenched ground or massive glass samples were introduced in platinum crucibles. Ignited alumina was chosen as the reference material. In order to investigate nucleation mechanisms (surface/bulk) occurring during reheating of the glass samples, the as quenched glasses A and C were crushed and sieved to obtain four different 200 mg size fractions (<20, 125–250, 400–800, 1600–2000 μm). For each of these glasses, massive samples were also prepared by remelting and quenching glass powders in the DTA crucible (≈6 mm-diameter). In this case, the number of surface crystallization sites is minimal. In order to attribute the main exothermic effects observed on DTA curves, 200 to 400 mg of as quenched glass samples with the same particle size as for DTA experiments were heated until the corresponding peak temperatures in a classical furnace at the same heating rate and then quenched to room temperature. The partially devitrified samples obtained were then characterized by XRD. DTA measurements were also performed using 100 mg of glass A (particle size <20 μm) and glass C (particle size 125–250 μm) with various heating rates α: 1, 5, 10, 20, 30, 40 and 50°C · min^{-1} (this last heating rate was not used for glass C). Discrepancies between these values and the true heating rates were only observed for the highest rates ($\alpha \geq 30$°C · min^{-1}) but the temperature evolution remains strictly linear with time. The true α values were considered for the kinetic study. The evolution of T_p (exothermic peak temperature) values with α was used to extract crystallization activation energies E_c, using the methods developed for non-isothermal crystallization studies by Matusita and Sakka [5, 6] for an interface-controlled crystal growth rate and by Macfarlane *et al.* [7] for diffusion controlled crystal growth rate. The n (Avrami constant) and m (crystal growth dimensionnality) numerical factors occurring in these methods are known to depend on crystallization mechanisms. They are summarized in Table II [8]. It must be underline that a meaningful activation energy can be obtained from these methods only when the crystallization mechanism is known precisely. The most probable n and m values associated with the crystallization of the different phases observed in this study, were deduced from the results of isothermal heat treatments reported in [4] (for the nucleation and crystal

TABLE II Values of n (Avrami constant) and m (crystal growth dimensionality) constants for various crystallization mechanisms [8]

Nucleation process	Number of nuclei	Crystal growth rate[a]	n	m
Surface	Constant	Constant	1	1
		Proportional to $t^{-1/2}$	0.5	0.5
Bulk	Constant	Constant		
		3-dimensional	3	3
		2-dimensional	2	2
		1-dimensional	1	1
Bulk	Constant	Proportional to $t^{-1/2}$		
		3-dimensional	1.5	1.5
		2-dimensional	1	1
		1-dimensional	0.5	0.5
Bulk	Inversely proportionnal to the heating rate	Constant		
		3-dimensional	4	3
		2-dimensional	3	2
		1-dimensional	2	1
Bulk	Inversely proportionnal to the heating rate	Proportional to $t^{-1/2}$		
		3-dimensional	2.5	1.5
		2-dimensional	2	1
		1-dimensional	1.5	0.5

[a]When crystal growth rate is proportional to $t^{-1/2}$, the mechanism is diffusion controlled whereas, when crystal growth rate is constant with time, the mechanism occurring can be controlled either by interface reaction or by diffusion. This latter case can be encountered for dendritic and spherullitic morphologies for instance [19, 20, 32].

growth mechanisms) and from DTA studies with different particle sizes (for the nucleation mechanism).

3. Non-isothermal devitrification study by DTA

Because of some significant differences observed on DTA curves between glass A on the one hand and glasses B and C on the other hand, the differential thermal analysis of glass A is treated separately. Moreover, glass A corresponds to the basic composition on which all current French investigations rely for the development of zirconolite-based glass-ceramics. This is why first emphasis is given on glass A before presenting DTA results concerning glasses B and C.

3.1. Differential thermal analysis of glass A

3.1.1. Effect of particle size

DTA runs were performed on four different size fractions (<20, 125–250, 400–800 and 1600–2000 μm) of glass A and on a massive sample. The DTA curves recorded using a constant heating rate of $10°C \cdot min^{-1}$ are showed in Fig. 1:

- Two relatively wide exothermic effects (referred as C2 and C3 on the figure) are detected for particle size samples lower than 1600 μm. The position (T_p), maximum height (δT_p) and width (ΔT_p) of these DTA peaks strongly change with the size fraction (Fig. 2a–c). For the coarsest samples (1600–2000 and 6000 μm), the peak T_p(C3) is too weak to be detected and it is hidden by the very wide thermal effect C2.
- A wider and weaker exothermic effect (referred as C1 on the figure) is observed in the temperature range 850–950°C before the effect C2, for size fractions lower than 400 μm. A displacement of this effect towards high temperature and a δT_p decrease are observed between the particle sizes <20 and 125–250 μm. This effect is not detected for higher size fractions (≥400 μm).
- An intense endothermic effect with two poorly resolved peaks is detected near 1260°C. The location and width of this effect do not significantly change with particle size. However, its intensity decreases for the massive sample.

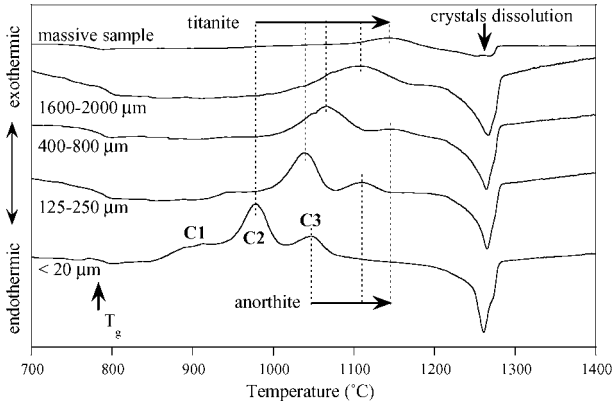

Figure 1 DTA curves for different size fractions and for a massive sample of glass A (heating rate: $10°C \cdot min^{-1}$, sample weight ≈ 200 mg).

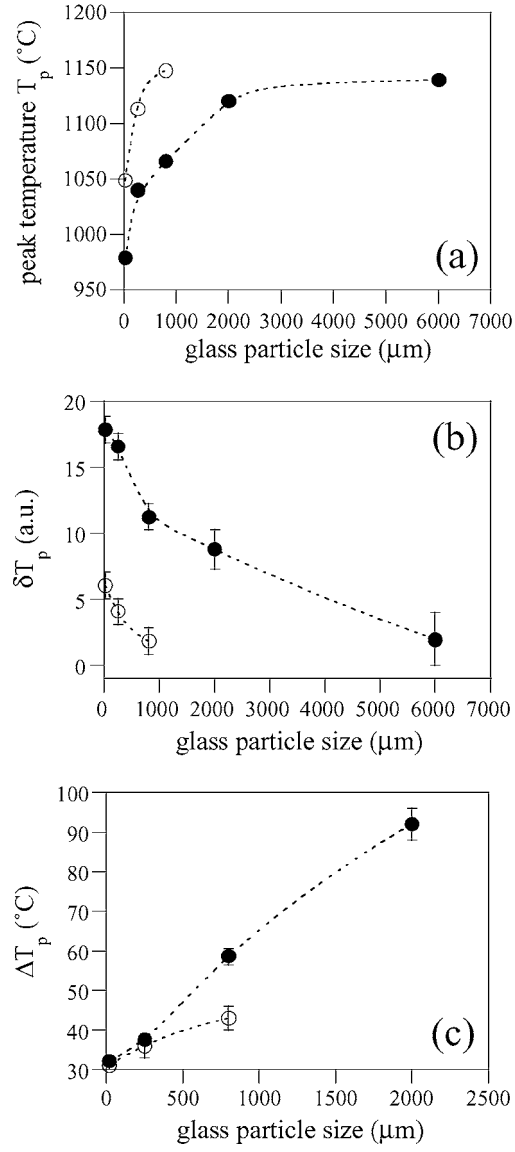

Figure 2 Evolution of exothermic DTA peaks (C2(●) and C3(○)) with size fraction (glass A) from Fig. 1 (heating rate: $10°C \cdot min^{-1}$): (a) evolution of the peak temperature T_p, (b) evolution of the maximum height δT_p, and (c) evolution of the width at half-peak maximum ΔT_p. Abscissa corresponds to the highest particle size of each fraction.

All these results show that the three exothermic effects (C1, C2 and C3) are very affected by the total surface area of glass samples. The corresponding phenomena (crystallization as showed below) are thus mainly initiated at the particle surfaces. On the contrary, if internal transformations were dominant, only weak modifications of DTA peaks should have been observed.

Indeed, it is known that:

- δT_p is generally proportional to the total number of nuclei (internal and surface nuclei formed either during the glass quenching or the DTA run) present in the glass sample [9, 10] and to the maximum crystallization rate [11]. Hence, for predominant surface nucleation, δT_p should diminish with increasing the particle size because the total number of surface nuclei decreases. Fig. 2b clearly indicates that δT_p(C2) and δT_p(C3) follow such an evolution.

– T_p generally increases with particle size for crystallization regulated by surface nucleation [12, 13]. Such an evolution is observed for the three exothermic peaks observed for glass A (Figs 1 and 2a). The displacement of T_p with size fraction can be explained by the following equation [14]:

$$\ln N = E_c/RT_p + \text{constant} \qquad (1)$$

where N is the concentration of bulk and surface nuclei, E_c is the crystallization activation energy and R is the gas constant. This equation shows that the greater the number of nuclei, the lower the crystallization peak temperature T_p. Consequently, a higher concentration of surface or bulk nuclei helps crystallization and a decrease of T_p is observed [13]. However, several references [9, 15] consider that the evolution of T_p with particle size is rather due to an indirect effect associated with an increasing heat transfer resistance when the size fraction increases. Nevertheless, for the glasses studied in this work, it will clearly show that exothermic peaks associated with surface crystallization displace to higher temperature, whereas for bulk crystallization the DTA peaks remain almost unchanged when the particle size increases (see below).

– ΔT_p increases with particle size for surface crystallization (Fig. 2c). This can be explained by considering the equation established by Augis and Bennet [16] which gives the relation between n (Avrami parameter), E_c , T_p and ΔT_p:

$$n = (2.5/\Delta T_p)\left(RT_p^2/E_c\right) \qquad (2)$$

Equation 2 shows that if the crystallization mechanism does not change with particle size (n and E_c thus remaining constant), T_p and ΔT_p must show opposite evolutions. Consequently, as T_p is displaced towards higher temperature with particle size, the exothermic effect becomes wider (ΔT_p increases).

So, all these points agree to conclude that the three exothermic effects (C1, C2 and C3) are associated with surface crystallization phenomena.

In order to identify more precisely the origin of the exothermic effects observed for glass A, heat treatments were performed for the <20, 125–250 and 400–800 μm particle size samples at the corresponding T_p values for 10 min. XRD patterns of the quenched samples were recorded and the results obtained for <20 μm particle size sample are showed in Fig. 3. Study of the XRD patterns shows that:

(i) The most intense exothermic peaks T_p(C2) and T_p(C3) are respectively due to titanite (nominally $CaTiSiO_5$) and anorthite (nominally $CaAl_2Si_2O_8$) crystallization from sample surface after heterogeneous nucleation (Figs 3b and c). This is in accordance with SEM observations [4]. The crystallization sequence observed during heating (1st-titanite and 2nd-anorthite) seems to indicate that anorthite begins to grow in the residual glass remaining between the elongated titanite crystals.

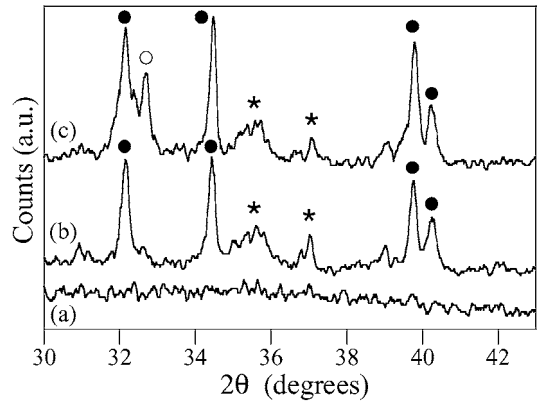

Figure 3 XRD patterns of glass A heated up to $T_1 = 917°C$ (a), $T_2 = 978°C$ (b) or $T_3 = 1049°C$ (c). Heating rate $10°C \cdot min^{-1}$, particle size <20 μm. The samples were kept for 10 min at the corresponding temperatures and were then quenched to room temperature. (●: titanite, ○: anorthite, ∗: defect-fluorite or/and zirconolite).

(ii) The small and wide exothermic effect C1 is probably not due neither to titanite nor anorthite crystallization. Although no diffraction peak is observed for the samples heat-treated in the temperature range of the first effect C1 (Fig. 3a), Fig. 3b shows for the sample heated at T_p(C2) some small broad lines, in addition to the main ones of titanite, which can be attributed to a mixture of two coexisting crystalline phases: zirconolite and defect-fluorite (defect-fluorite structure phase can be considered as a highly disordered zirconolite which forms at lower temperature than 1000°C [4]). So, the exothermic effect C1 is probably associated with a weak crystallization of defect-fluorite from sample surface. This result will be reinforced below by the DTA study of glass B and C: these glasses have a strong exothermic peak F associated with defect-fluorite crystallization in the same range of temperature as C1, though this peak F is due to an internal crystallization contrary to C1 for glass A.

It is important to underline that no thermal effect associated with crystallization events in the bulk of the glass was detected by DTA for glass A even for the massive sample (Fig. 1). This is due to the low zirconolite nucleation and crystal growth rates in glass bulk in comparison with the ones of silicate phases growing from glass surface. Thus during DTA runs, the energy involved in zirconolite crystallization in the bulk is too weak to be detected. However for glasses B and C, an exothermic effect associated with zirconolite crystallization will be observed (see below).

The endothermic effect observed near 1260°C is probably associated with titanite and anorthite dissolution in the residual glass. The fact that this effect is smaller for the massive sample (Fig. 1) indicates that the amount of crystalline phase formed during DTA runs is lower than for ground samples. In this case, silicate phases nucleate only on the crucible surface and on the air-melt interface. It can be noticed that the dissolution temperature range is lower than the titanite (1382°C [17]) and anorthite (1553°C [18]) melting points.

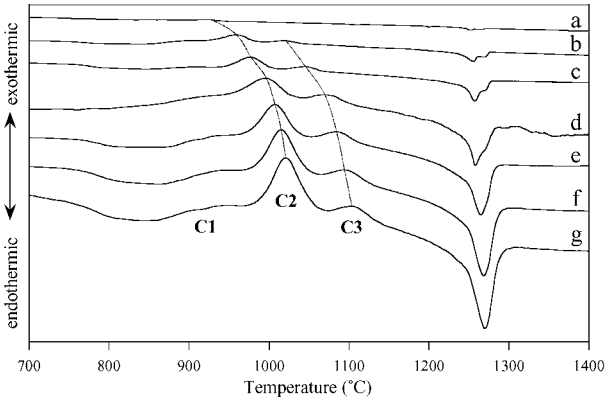

Figure 4 DTA curves for different heating rates: $1°C \cdot min^{-1}$ (a), $5°C \cdot min^{-1}$ (b), $10°C \cdot min^{-1}$ (c), $20°C \cdot min^{-1}$ (e), $30°C \cdot min^{-1}$ (f), $40°C \cdot min^{-1}$ (f) and $50°C \cdot min^{-1}$ (g). (Glass A, particle size $<20\ \mu m$).

3.1.2. Effect of heating rate

For glass A, the only crystal growth activation energies E_c which can be calculated from DTA curves are the ones of titanite and anorthite but not the one of defect-fluorite/zirconolite. Nevertheless, it is interesting to further characterize titanite and anorthite crystallization processes by evaluating E_c. Indeed, these silicate phases can have a crucial role on the long-term behavior of glass-ceramics if the devitrification thermal treatment is badly controlled. Should that arise, the crystallized surface layer could occupy a significant fraction of glass-ceramics and the silicate phases should then be taken into account to evaluate the chemical durability of the wasteform. Moreover, as titanite and anorthite form on the surface of glass-ceramics, these crystalline phases together with the surface residual glass would always be the first phases leached by groundwater in the storage repositories.

DTA curves were recorded for glass A at various heating rates ranging from 1° to $50°C \cdot min^{-1}$ (Fig. 4). The 20 μm size fraction was chosen for this study because in this case the exothermic effects C2 and C3 are well resolved (Fig. 1). A progressive displacement of T_p(C2,C3) towards higher temperature and an increase of δT_p(C2,C3) were observed with increasing the heating rate α. The variation of T_p with α (Table III) was used to extract E_c values using the modified form of the Kissinger equation:

$$\ln\left(\alpha^n / T_p^2\right) = -mE_c/RT_p + \text{constant} \qquad (3)$$

and the modified form of the Ozawa equation:

$$\ln \alpha = -mE_c/nRT_p + \text{constant} \qquad (4)$$

TABLE III DTA peak temperature of titanite (T_p(C2)) and anorthite (T_p(C3)) crystallization as a function of the heating rate (glass A, particle size $<20\ \mu m$)

Heating rate α ($K \cdot s^{-1}$)	T_p(C2) (K)	T_p(C3) (K)
0.0166	1195	–
0.0866	1231	1291
0.1766	1249	1318
0.3583	1267	1343
0.5466	1280	1356
0.7250	1288	1365
0.9233	1295	1373

where n is the Avrami constant and m is the crystal growth dimensionnality. These equations were established by Matusita and Sakka [5, 6] assuming that:

– nucleation does not occur during crystal growth
– crystal growth is interface controlled (u does not depend on time for a given temperature).

However, similar equations were also obtained by Macfarlane *et al.* [7] for diffusion controlled crystal growth. This generally occurs when the composition of the crystals and the composition of the parent glass are different. In this case the crystal growth rate u generally decreases with time for a given temperature according to $u \propto t^{-1/2}$ [19]. However, for crystals exhibiting dendritic or spherulitic morphologies, growth rate is generally constant [19, 20].

SEM and DTA results show that titanite and anorthite elongated crystals nucleate from sample surface [4]. Crystals morphology (dendritic for titanite and needle-like for anorthite) are in accordance with a constant crystal growth rate. Moreover, because of the high surface nucleation rate, it can be assumed that all the surface nuclei are formed before crystal growth. Hence no new nuclei form during growing. Equations 3 and 4 can thus be used with $n = m = 1$: surface crystallization with u constant (Table II). It can be noticed that in this case, the modified Equations 3 and 4 are the same as the classical Kissinger and Ozawa equations [5]. Fig. 5a and b show respectively the Kissinger and Ozawa plots for the two crystalline phases. These curves were fitted using linear regression and activation energies were extracted (Table IV). The E_c values obtained using either the Kissinger or the Ozawa equations give very similar results. This is not surprising

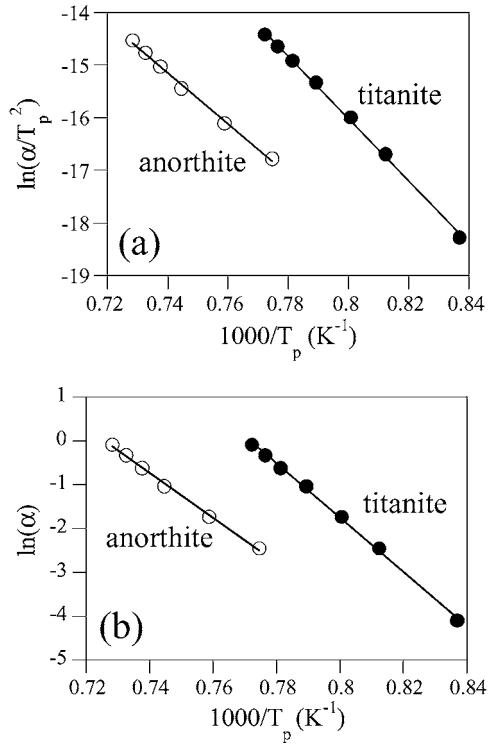

Figure 5 Kissinger (a) and Ozawa (b) plots corresponding to the surface crystallization for glass A (particle size $<20\ \mu m$).

TABLE IV Titanite and anorthite crystal growth activation energies deduced from linear regressions for Ozawa and Kissinger type plots ($n = m = 1$) (Fig. 5). Correlation coefficients are given in brackets

Plot type	Activation energy for titanite crystallization ($kJ \cdot mol^{-1}$)	Activation energy for anorthite crystallization ($kJ \cdot mol^{-1}$)
Ozawa	514 (0.999)	427 (0.998)
Kissinger	493 (0.999)	405 (0.998)

because these two equations are equivalent for a small T_p range [21]. The E_c value associated with anorthite is lower than the one associated with titanite. This difference could be partly due to a weak decrease of the viscous flow activation energy of the melt between the temperature ranges of titanite (T_p: 922–1022°C) and anorthite (T_p: 1018–1100°C) crystallization.

Comparison of these results with the ones reported by Hayward *et al.* [21] for titanite crystal growth in a Na_2O-Al_2O_3-CaO-TiO_2-SiO_2 parent glass indicates that, in this latter case, crystal growth occurs between 810°–910°C (particle size <37 μm) with $E_c = 461 \pm 57$ $kJ \cdot mol^{-1}$ and $E_c = 480 \pm 57$ $kJ \cdot mol^{-1}$ (values respectively obtained from the Ozawa and Kissinger type plots). These values are only slightly lower than the ones obtained in this study (Table IV). These weak differences are probably due in part to different flow activation energies between the two corresponding melts.

3.2. Differential thermal analysis of glasses B and C

3.2.1. Comparison with glass A

Comparison of the DTA curves recorded for glasses A, B and C (size fraction 125–250 μm) indicates that there are great differences between the three samples, especially in the low temperature range (Fig. 6):

– Two new relatively sharp exothermic peaks referred as F ($T_p = 875$°C) and Z ($T_p = 1022$°C) are detected for glass C. These effects are also observed for sample B but peak F is displaced towards higher temperature ($T_p = 952$°C) and becomes wider and less intense whereas peak Z remains almost unchanged ($T_p = 1029$°C). It is interesting to notice that the very wide and weak effect C1 observed for sample A occurs in the same temperature range as peak F for sample B.
– Effects C2 and C3 attributed to surface crystallization of titanite and anorthite respectively for glass A, are displaced to higher temperature and are not resolved for samples B and C.
– Endothermic effects previously attributed to titanite and anorthite dissolution in residual glass are still present ($T_p \approx 1260$°C). However, a new and weak endothermic effect (D in Fig. 6) is observed at high temperature (T_p: 1290°–1320°C) for glasses B and C. This effect seems to be correlated with the occurrence of peaks F and Z.

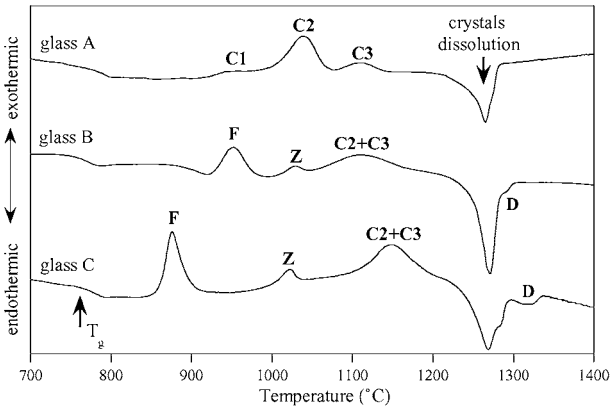

Figure 6 DTA curves of as-quenched glasses A, B and C (heating rate: $10°C \cdot min^{-1}$, particle size 125–250 μm).

Using the same method as for sample A, peaks F and Z were identified after thermal treatments at different temperatures for samples B and C. The XRD patterns reported in Figs 7 and 8 indicate that:

– The first exothermic peak F can be attributed to the crystallization of the defect-fluorite phase yet reported in [4] which corresponds to a totally cationic disordered zirconolite (cubic structure). The

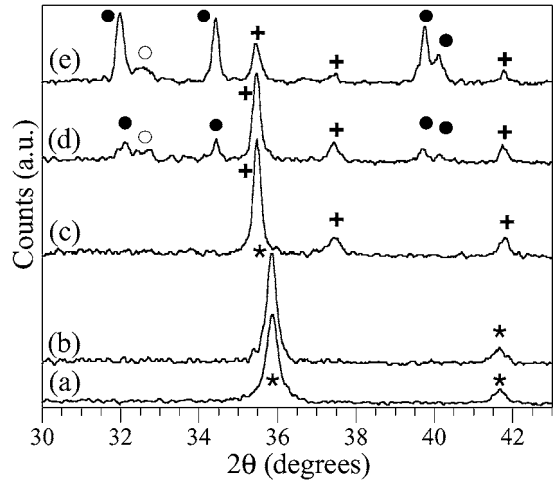

Figure 7 XRD patterns of glass C heat treated up to: 890°C (a), 950°C (b), 1022°C (c), 1050°C (d) and 1150°C (e). Heating rate $10°C \cdot min^{-1}$, particle size 125–250 μm. Samples were kept for 12 min at these temperatures and were then rapidly cooled to room temperature. (●: titanite, ○: anorthite, ∗: defect-fluorite, +: zirconolite).

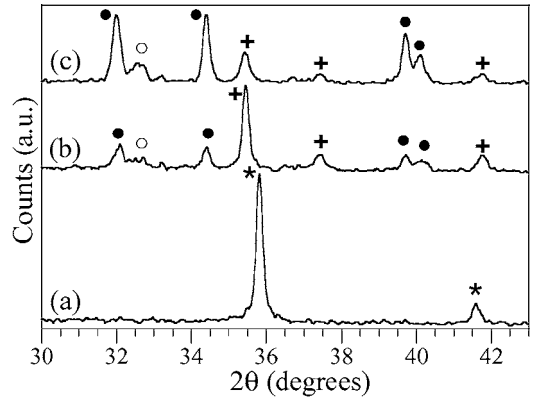

Figure 8 XRD patterns of glass B heat treated up to: 972°C (a), 1068°C (b) and 1130°C (c). Heating rate $10°C \cdot min^{-1}$, particle size 125–250 μm. Samples were kept 12 min at these temperatures and were then rapidly cooled to room temperature. (●: titanite, ○: anorthite, ∗: defect-fluorite, +: zirconolite).

detection of this crystalline phase during DTA run is in accordance with the results obtained after a 2 h isothermal treatment at $T_c = 860°C$ performed on glass C [4].

– The second but less intense exothermic effect Z can be attributed to the irreversible transformation of the previous defect-fluorite phase into zirconolite-2M (cationic reordering). The defect-fluorite phase can be thus considered as an intermediate disordered phase with a cubic structure which grows at $T_p(F)$ and transforms irreversibly into zirconolite-2M at higher temperature $T_p(Z)$. This crystallization and phase transformation sequence is also in accordance with the results of the isothermal heat treatment study of glass A [4]: the defect-fluorite phase is observed for $T_c < 1000°C$ and is totally transformed into zirconolite for $T_c \geq 1000°C$. However, because of its low nucleation rate in the bulk of glass A, no thermal effect is detected neither for defect-fluorite crystallization nor for its transformation into zirconolite. The effect C1 detected for glass A was attributed to defect-fluorite formation only from sample surface.

It is interesting to notice that a similar evolution with temperature (crystallization followed by phase transformation) has already been observed by Vance *et al.* [22] for an amorphous zirconolite alkoxide precursor using DTA and isothermal treatments. These authors observed an exothermic peak ($T_p = 750°C$) attributed to defect-fluorite phase crystallization followed by a weak exothermic peak at higher temperature ($T_p = 1025°C$) associated with the defect-fluorite → zirconolite transformation. This last temperature is very similar to the one found in this study, $T_p(Z)$: 1022°–1029°C. Moreover, a DTA exothermic peak at $T_p = 690°C$ was also observed by Weber *et al.* [23] during the recrystallization of a sample of curium doped metamict zirconolite. These authors attributed this effect to the crystallization of a pseudo-cubic intermediate phase. During their DTA study of a natural metamict zirconolite sample, Lumpkin *et al.* [24] detected also an exothermic effect attributed to the crystallization of a defect-fluorite structure at $T_p = 780°C$. The different authors who worked on metamict zirconolite did not perform their DTA runs at temperature high enough to be able to detect the transformation of defect-fluorite into zirconolite. However, it is important to underline that the DTA peak temperature associated with defect-fluorite crystallization ($T_p(F)$) strongly depends on the sample studied. This seems to be less the case for $T_p(Z)$ comparing the results of this study with the one of Vance *et al.* [22].

Moreover, supplementary remarks can be made:

(i) The enthalpy of defect-fluorite crystallization $|\Delta H(F)|$ (proportional to the peak area) from either a silicate glass (this study, Fig. 6) or from an amorphous alkoxide precursor [22], is always higher than the enthalpy associated with the defect-fluorite → zirconolite transformation $|\Delta H(Z)|$. This result can be easily explained because of the small enthalpy difference between zirconolite and defect-fluorite due only to cationic reordering whereas a deep reorganization (and consequently a higher transformation enthalpy) of the amorphous precursor (glass or amorphous precipitate) is necessary for defect-fluorite crystallization.

(ii) Different factors may influence the exothermic peaks shape and position for the defect-fluorite crystallization:

– Nuclei concentration differences between samples B and C due to different nucleation rates [4] may explain the decrease of $\delta T_p(F)$ and the increase of $\Delta T_p(F)$ and $\Delta T_p(Z)$ observed in Fig. 6 for glass B. Moreover, the increase of the defect-fluorite crystallization peak intensity $\delta T_p(F)$ and its displacement towards lower temperature for glass C (Fig. 6) show that glass stability decreases in the order glass A > glass B > glass C. This is in accordance with the results obtained by isothermal treatments [4] which indicate that zirconolite nucleation rate increases between glass A and glass C.
– The higher $T_p(F)$ values (>875°C) observed in this study in comparison with the values reported in literature either for a metamict ($T_p(F)$: 690°–780°C [23, 24]) or an alkoxide precursor ($T_p(F) = 750°C$ [22]) can be explained because defect-fluorite nucleation and growth rates for a silicate glassy precursor becomes only significant when the viscosity of the supercooled liquid is low enough to allow diffusion, that is to say for $T > T_g = 760°C$. Besides, there are less diffusion problems for the metamict and the alkoxide precursor that only contain the constitutive oxides of zirconolite than for the glass-ceramic in which zirconolite is only a dilute component. Moreover, from the structural results reported in literature, one can think that the formation of the crystalline state is easier from metamict zirconolite than from a glass. Indeed, EXAFS studies performed on natural metamict zirconolite samples showed that Zr^{4+} ions are mainly 7-coordinated as in zirconolite crystals and with nearly identical bond lengths [25]. Ti K-edge XANES studies performed on the same amorphous samples showed that Ti^{4+} ions are mainly fivefold coordinated with trigonal pyramids sites. Such a titanium site exists also in crystalline zirconolite [26]. On the contrary EXAFS studies performed on various silicate glass samples indicate that Ti^{4+} and Zr^{4+} ions local environments are different from their environment in zirconolite (titanium is mainly 5-coordinated as square pyramids [27] and zirconium is mainly 6-coordinated [28, 29]). Although no such structural studies were performed on the parent glasses A, B or C, these bibliographic results show that, contrarily to glasses, the local environment of Ti^{4+} and Zr^{4+} ions in amorphous zirconolite is very similar to the one in crystallized zirconolite. Consequently, at least for titanium and zirconium ions, crystallization needs less reorganization for amorphous zirconolite than for glasses.

Thermal treatments performed in the C2 + C3 temperature range (1050°–1150°C) for samples C confirmed that this effect is due to titanite and anorthite crystallization as for sample A (Figs 7d and e and 8b and c). It is interesting to notice that the intensity of

zirconolite XRD lines decreases when titanite and anorthite form. This evolution can be explained by the occurrence of a reaction between these crystals and zirconolite [30]. Furthermore, this kind of reaction could partly explain the progressive displacement towards higher temperature of C2 and C3 effects when composition changes (Fig. 6) from A to C because of the higher amount of zirconolite nuclei which form near the surface and which disturb silicate phases crystallization.

3.2.2. Effect of particle size

Attribution of C1, C2 and C3 exothermic peaks was confirmed by recording DTA curves for four size fractions (<20, 125–250, 400–800 and 1600–2000 μm) and for a massive sample of as quenched glass C (Fig. 9). Displacement of the C2 + C3 effects towards higher temperatures with increasing the particle size (Fig. 10a) shows that the corresponding crystallization processes are initiated by the surface, which is in accordance with SEM observations [4]. Moreover, as for glass A (Fig. 1), a decrease of the intensity of the corresponding dissolution peaks ($T_p \approx 1260°C$) is observed for the highest size fraction. On the contrary, peaks F and Z do not significantly change with size fraction (Figs 9 and 10). This shows that defect-fluorite crystallization in glass C and its consecutive transformation into zirconolite are mainly bulk phenomena. This agrees with SEM and XRD observations reported in [4]: defect-fluorite crystals nucleate in the bulk and cationic ordering in these crystals (transformation into zirconolite) obviously do not depend on glass particle size. The slight decrease of the defect-fluorite crystallization peak width ΔT_p observed for the massive sample (Figs 9e and 10c) seems to indicate that a weak contribution of defect-fluorite surface crystallization occurs for ground samples. The small endothermic effect D is detected for all particle size samples ($T_p \approx 1320°C$) and is probably due to zirconolite crystals dissolution in the residual glass. It can be noticed that this dissolution temperature is lower than the ones reported in literature for pure zirconolite decomposition ($T \approx 1525°C$ [31]).

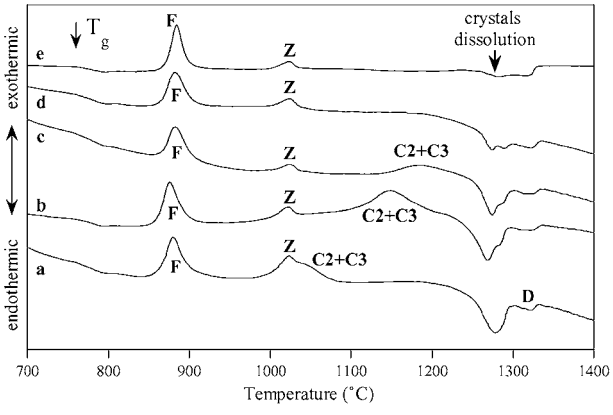

Figure 9 DTA curves for different size fractions of glass C (heating rate: $10°C \cdot min^{-1}$, sample weight $\approx$ 200 mg): <20 μm (a), 125–250 μm (b), 400–800 μm (c), 1600–2000 μm (d) and massive sample (e).

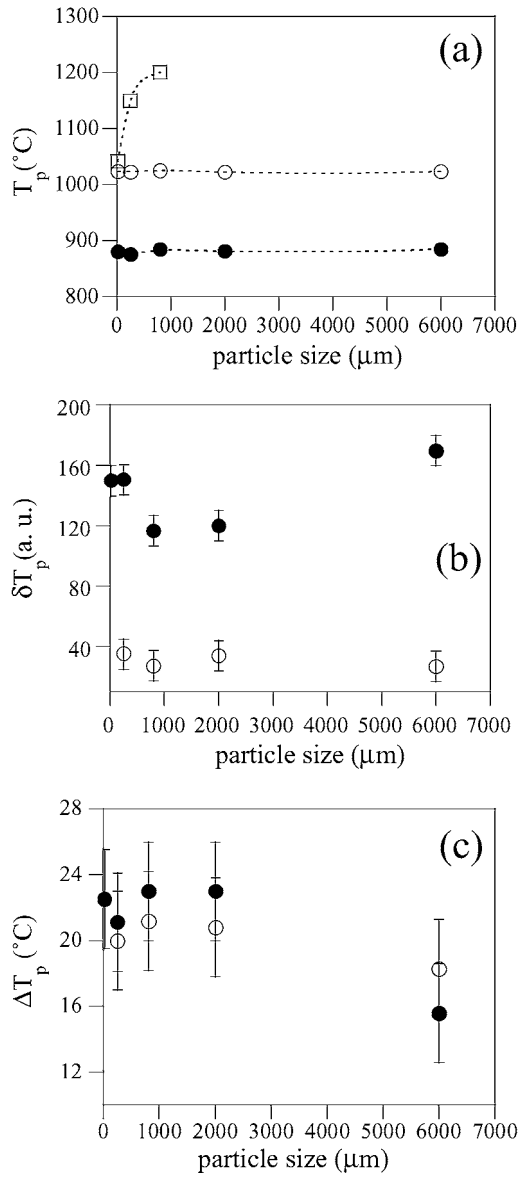

Figure 10 Evolution of exothermic DTA peaks (F(●), Z(○) and C2+C3(□)) with size fraction (glass C) from Fig. 9 (heating rate: $10°C \cdot min^{-1}$): (a) evolution of the peak temperature T_p, (b) evolution of the maximum height δT_p and (c) evolution of the width at half-peak maximum ΔT_p. Abscissa corresponds to the highest particle size of each fraction.

3.2.3. Effect of heating rate

Fig. 11 shows the evolution of DTA curves recorded for glass C at different heating rates ranging from 1 to $40°C \cdot min^{-1}$. The 125–250 μm size fraction was chosen for this study because in this case, the Z effect little interferes with the C2 + C3 effect (Fig. 9). A progressive displacement of T_p(F) and T_p(Z) towards higher temperature with α is observed (Table V). It was used to extract defect-fluorite crystallization (E_c(F)) and transformation into zirconolite (E_c(Z)) activation energies. However n and m parameters must be known in order to use either modified Kissinger or Ozawa equations. SEM studies reported in Part 1 of this work [4] showed that the defect-fluorite crystals nucleate mainly in glass bulk with a 3-dimensional growth. This was easily observed for glass A, for which the crystal density in bulk is not too high. The same 3-dimensional crystallization mode was assumed for glass C. Moreover, it was

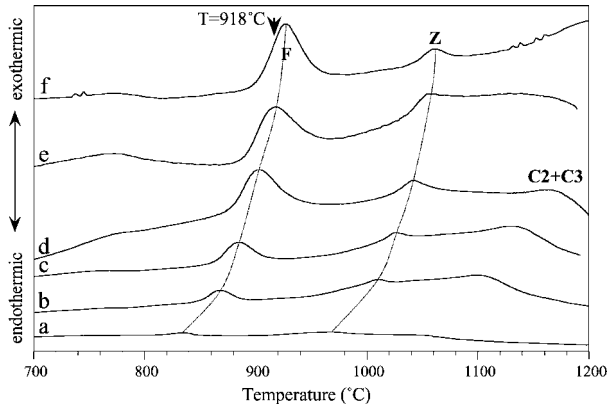

Figure 11 DTA curves for different heating rates (glass C, particle size 125–250 μm, sample weight $\approx$ 100 mg): $1°C \cdot min^{-1}$ (a), $5°C \cdot min^{-1}$ (b), $10°C \cdot min^{-1}$ (c), $20°C \cdot min^{-1}$ (d), $30°C \cdot min^{-1}$ (e) and $40°C \cdot min^{-1}$ (f).

showed that the defect-fluorite nucleation rate of glass A exhibits a narrow maximum at $T_{max} = 790°C$ [30]. Therefore, it can be assumed that no new nuclei are formed during defect-fluorite crystal growth (Fig. 11) and that the activation energy determined by DTA corresponds only to the activation energy for the crystal growth of defect-fluorite [12]. Furthermore, the nucleation rate of defect-fluorite in glass C is so fast that the number of nuclei formed during DTA runs can be considered as constant irrespective of the heating rate. Study of Table II shows that for such a situation, two possibilities exist for the n and m parameters: $n = 3$ and $m = 3$ (constant crystal growth rate) or $n = 1.5$ and $m = 1.5$ (crystal growth rate proportional to $t^{-1/2}$). The Avrami constant n can be deduced using the following equation [5, 7] which is a general form of the modified Ozawa equation for T not necessarily equal to T_p:

$$\ln \alpha = -(mE_c/nRT) - (1/n)\ln[-\ln(1-x)] + \text{constant} \quad (5)$$

which gives the evolution of x (amount of crystallized defect-fluorite) at the temperature T during a DTA run as a function of the heating rate α. x can be determined from DTA curves:

$$x = S/S_0 \quad (6)$$

where S_0 is the area under the DTA curve between the temperature at which crystallization starts (T_b) and the temperature at which crystallization is complete (T_e). S is the area of the DTA curve between T_b and the

TABLE V DTA peak temperature of defect-fluorite (T_p(F)) and zirconolite crystallization (T_p(Z)) as a function of the heating rate (glass C, particle size 125–250 μm)

Heating rate ($K \cdot s^{-1}$)	T_p(F) (K)	T_p(Z) (K)
0.016700	1107.0	1240.0
0.086700	1140.3	1284.0
0.17830	1157.5	1299.0
0.37000	1176.0	1315.0
0.56500	1190.8	1330.0
0.68330	1199.6	1334.0

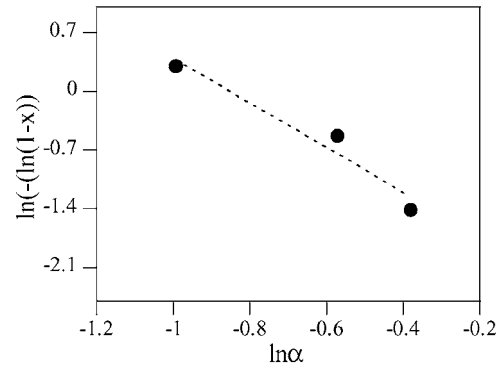

Figure 12 Evolution of $\ln[-\ln(1-x)]$ against $\ln\alpha$ for glass C at $T = 918°C$ (size fraction 125–250 μm).

arbitrarily fixed temperature T. In this case, Equation 5 leads to:

$$d(\ln[-\ln(1-x)])/d\ln\alpha = -n \quad (7)$$

Choosing $T = 918°C$ (Fig. 11), x was calculated for $\alpha = 20$, 30 and $40°C \cdot min^{-1}$ by plotting $\ln[-\ln(1-x)]$ against $\ln\alpha$. The plot obtained is showed in Fig. 12 with a linear fit giving $n \approx 2.6$. Between the two possibilities ($n = 3$ and $n = 1.5$) indicated in Table II for a bulk nucleation process with a constant number of nuclei, the $n \approx 2.6$ value appears closer to 3. Thus, defect-fluorite crystal growth rate seems to be constant. This can be understood because, as the crystal morphology is very likely to be dendritic, a constant crystal growth rate is expected even if the crystallization is intrinsically controlled by diffusion (incongruent crystallization) [19, 20, 32]. Therefore, $n = 3$ and $m = 3$ constants were chosen to extract E_c(F). Fig. 13a and b show

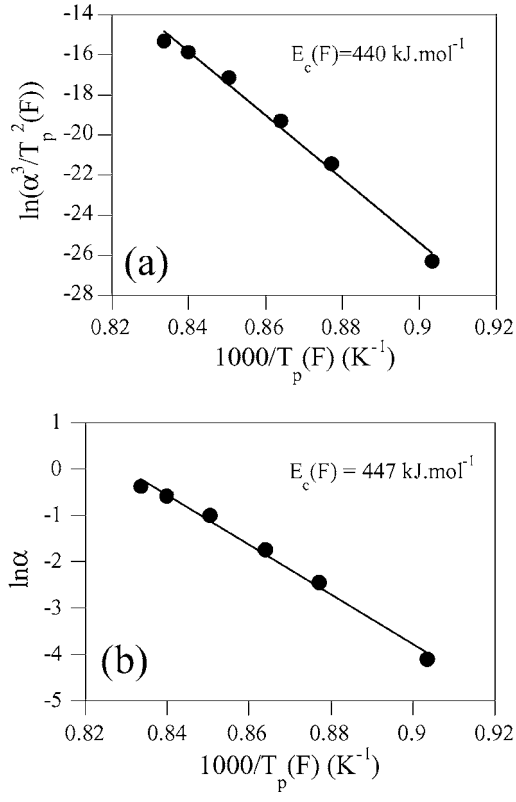

Figure 13 Modified Kissinger (a) and Ozawa (b) plots ($n = 3$, $m = 3$) corresponding to the defect-fluorite crystallization for glass C (particle size 125–250 μm).

TABLE VI Defect-fluorite and zirconolite crystal growth activation energies deduced from linear regressions for modified Ozawa and Kissinger type plots (Figs 13 and 14). Correlation coefficients are given in brackets

Plot type	Activation energy for defect-fluorite crystallization ($kJ \cdot mol^{-1}$)	Activation energy for zirconolite crystallization ($kJ \cdot mol^{-1}$)
Modified Kissinger ($n = 3, m = 3$)	440 (0.995)	–
Modified Ozawa ($n = 3, m = 3$)	447 (0.996)	–
Kissinger ($n = 1, m = 1$)	–	527 (0.998)
Ozawa ($n = 1, m = 1$)	–	549 (0.998)

respectively the modified Kissinger and Ozawa plots corresponding to these values. The calculated crystal growth activation energies using linear regression are respectively $E_c(F) = 440$ and $447\ kJ \cdot mol^{-1}$ (Table VI). The value determined with the modified Ozawa equation was lower than the activation energy obtained by Vance *et al.* [22] using the Ozawa equation ($n = m$) for defect-fluorite crystallization from an alkoxide amorphous precursor ($E_c(F) = 940\ kJ \cdot mol^{-1}$) but is close to their value $E_c(F) = 430\ kJ \cdot mol^{-1}$ deduced from isothermal measurements and considered by themselves as more probable. Furthermore, for a metamict zirconolite sample, Weber *et al.* [23] determined a crystallization activation energy $E_c \approx 560\ kJ \cdot mol^{-1}$ by DTA (Kissinger method, $n = m = 1$). These discrepancies between the activation energies reported in literature show that even for amorphous zirconolite, E_c depends on the preparation method and on the composition of the material (presence of impurities in natural samples). Furthermore, even if the two samples (metamict and alkoxide precursor) appear XRD amorphous, their degree of disorder are probably different.

Concerning defect-fluorite transformation into zirconolite-2M, it was assumed that it occurs also by a process of nucleation and growth as showed in reference [22]. In this case, because of the small defect-fluorite crystal size (<100 nm), it can be assumed that zirconolite crystallization starts from their surface towards their bulk and is controlled by interface reaction [22]. $n = m = 1$ constants were thus used to extract $E_c(Z)$. Fig. 14 shows the linearly fitted Kissinger and Ozawa plots for the exothermic effect Z. The activation energies obtained by the two methods give respectively $E_c = 527$ and $549\ kJ \cdot mol^{-1}$ (Table VI). Comparison can be made with the $E_c = 800\ kJ \cdot mol^{-1}$ value determined by Vance *et al.* [22] using the Ozawa equation ($n = m$) and the $E_c = 330\ kJ \cdot mol^{-1}$ value determined using isothermal measurements and considered as more probable by these authors. Whereas the defect-fluorite → zirconolite transformation occurs in the same temperature range 1020°–1030°C for the two samples (glass C and alkoxide precursor), differences are observed between their $E_c(Z)$ values. The origin of these discrepancies are not clear but may be due to microstructural and composition differences between the zirconolite crystals grown in glass C and the ones formed from a pure alkoxide precursor [22].

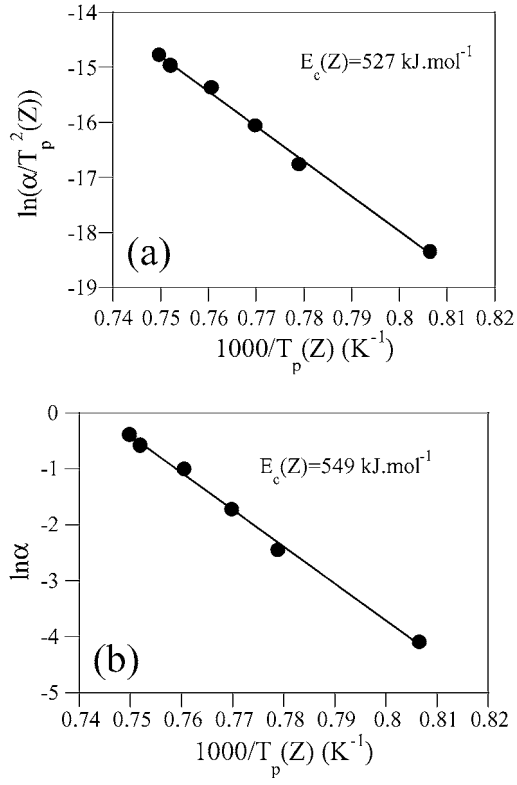

Figure 14 Kissinger (a) and Ozawa (b) plots ($n = 1$, $m = 1$) corresponding to the defect-fluorite transformation into zirconolite for glass C (particle size 125–250 μm).

3.3. Crystallization of the melt followed by DTA

After DTA runs, only a slight crystallization is observed in DTA crucibles for glass A and no significant exothermic effects are detected on the DTA curves during cooling (from 1450°C to room temperature with a $10°C \cdot min^{-1}$ cooling rate). However, for glasses B and C, the samples recovered after DTA runs (cooling rate $10°C \cdot min^{-1}$ from 1600°C) exhibit large crystals on their surface. The size of these crystals—which can be larger than 1 mm for some of them- indicates that they have grown from only a small number of nuclei on the crucible surface or on the air-melt interface. Correlatively, large and wide exothermic effects, referred as B ($T_p(B) \approx 1245°C$) and Z ($T_p(Z) \approx 1040°C$) in Fig. 15b, are detected on DTA curves during cooling of sample C. These effects are less intense for glass B. The intensity and width of these two peaks vary from one test to another for glass C. Moreover the intensity of peak B was showed to depend on the nature of the DTA crucible (alumina or platinum). All these observations are in accordance with a heterogeneous nucleation process occurring on a small number of nuclei which may vary from one sample to another. Fig. 16 shows an example of SEM micrographs for a sample of glass C recovered at room temperature after a DTA run. Two kinds of crystals were observed and identified:

– Very large crystals which appear in white on SEM images and show dendritic shapes with perpendicular crystal growth directions. EDX and XRD studies indicate that these crystals correspond to ZrO_2 (baddeleyite) which have incorporated a small amount of

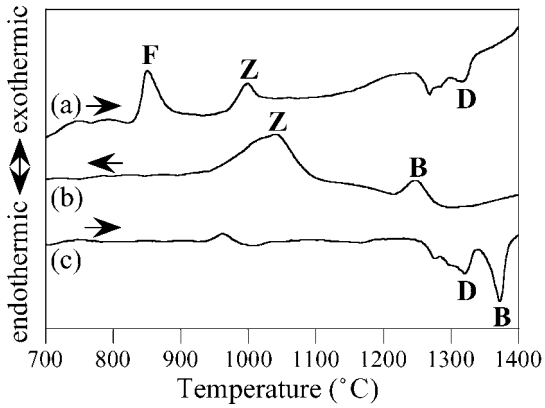

Figure 15 DTA curves recorded for glass C: (a) first heating ($10°C \cdot min^{-1}$) to 1600°C, (b) cooling ($10°C \cdot min^{-1}$) to room temperature, (c) second heating ($10°C \cdot min^{-1}$) to 1600°C (Sample weight ≈ 300 mg, massive sample). Arrows on the figure indicated heating or cooling.

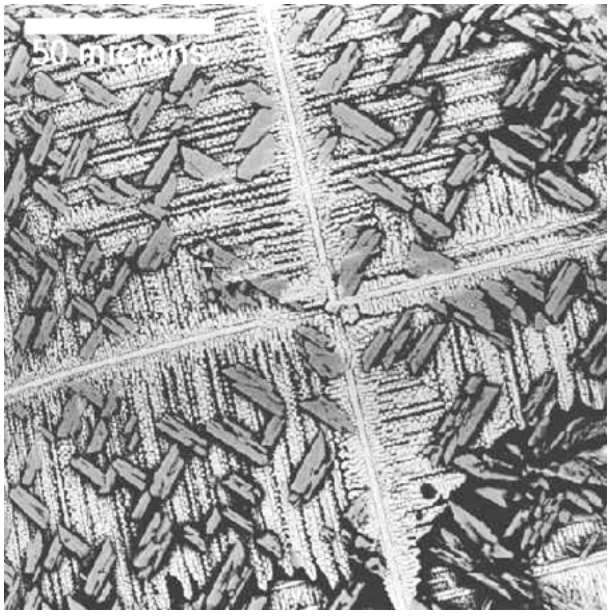

Figure 16 Back-scattered SEM micrographs of glass C after a DTA run (heating rate $10°C \cdot min^{-1}$ to 1600°C and cooling to room temperature at the same rate). Baddeleyite crystals are white and zirconolite crystals are light gray.

TiO_2. Notably, samples were quenched at 1200°C to room temperature after cooling the melt from 1650°C. The results obtained show that growth of ZrO_2 is responsible for the first exothermic effect (B in Fig. 15b). The strong endothermic peak detected at $T_p = 1372°C$ during reheating (Fig. 15c) is probably associated with ZrO_2 dissolution in the residual glass. This effect was not observed during the first heating (Fig. 15a) where only titanite, anorthite and zirconolite dissolution occurred.

– Smaller crystals which appear in gray on SEM images and which show a lath-like morphology similar to the one observed for zirconolite crystals grown at high temperature in glass A [4, 33]. EDX and XRD studies confirmed that these crystals corresponded to zirconolite and were responsible for the second exothermic effect (Z in Fig. 15b). It is interesting to notice that the zirconolite crystals have essentially grown on the large ZrO_2 crystals yet formed. Moreover, these crystals are not randomly oriented compared with the main crystal growth directions of baddeleyite (Fig. 16). This phenomenon is probably due to epitaxial relations between the two crystalline phases which favor heterogeneous nucleation of zirconolite on baddeleyite. The existence of such crystallographic relations is not surprising because the two structures can be considered as defect-fluorite structural derivatives. Moreover, a careful study of SEM images shows that zirconolite crystals grow at the expense of ZrO_2 crystals which are consequently progressively consumed during cooling as confirmed by XRD. This result indicates that baddeleyite crystals firstly nucleate and grow at low undercooling (and thus control the liquidus temperature of the melt) but become unstable versus zirconolite for higher undercooling.

Therefore, slow cooling of highly TiO_2-ZrO_2 enriched melts firstly lead to ZrO_2 crystallization ($T < 1300°C$, Fig. 15). For lower temperatures this phase transforms into zirconolite reacting with the residual supercooled liquid. This crystallization sequence observed during the cooling of melt C is in accordance with the results concerning glass A devitrification reported in [34]: zirconolite is the only crystalline phase that forms in the bulk for $1000° \leq T_c \leq 1200°C$ whereas baddeleyite crystals grow for $T_c \geq 1250°C$ at the expense of zirconolite (T_c: crystal growth temperature).

4. Conclusions

From the DTA study of (TiO_2-ZrO_2)-rich glasses performed for different particle size fractions and different heating rates, the following main conclusions can be drawn:

1. The determination of nucleation mechanisms (bulk or surface) by recording DTA curves for different glass particle sizes are in good accordance with the results deduced from isothermal treatment reported in [4]: defect-fluorite (precursor phase of zirconolite) nucleates in the bulk of the glass whereas titanite and anorthite nucleate on the surface.

2. For the lowest TiO_2 and ZrO_2 concentrations, only exothermic effects associated with the crystallization of titanite and anorthite from glass particles surface are clearly detected respectively at $T_p = 980°$ and 1050°C for the smallest size fraction (<20 μm). The activation energy E_c associated with crystal growth of titanite and anorthite was determined using the Kissinger or Ozawa methods ($n = m = 1$, surface nucleation with a constant crystal growth rate). The E_c values obtained by these two methods are very similar. The Kissinger method gives respectively $E_c = 493$ and $405\ kJ \cdot mol^{-1}$ for titanite and anorthite. The fact that no clear exothermic effect associated with zirconolite (or defect-fluorite) crystallization is detected during DTA runs can be explained by a low bulk crystallization rate for this glass composition.

3. For higher TiO_2 and ZrO_2 concentrations, two new exothermic effects associated with phenomena occurring in the bulk of the glasses are detected. The first one (near 880°C) is due to the crystallization of the defect-fluorite phase that has already been observed after isothermal treatment at 860°C [4]. The second one (occurring at higher temperature near 1020°C) is due to the transformation of the defect-fluorite phase into zirconolite by cationic ordering. Activation energy associated with defect-fluorite crystallization was determined for the (TiO_2, ZrO_2)-richest glass using the modified Kissinger (440 $kJ \cdot mol^{-1}$) and Ozawa (447 $kJ \cdot mol^{-1}$) methods with $n = 3$ and $m = 3$ (3-dimensional growth controlled by diffusion with a constant crystal growth rate). Defect-fluorite transformation into zirconolite is assumed to occur by nucleation and growth from crystal surface and $E_c = 527$ $kJ \cdot mol^{-1}$ was obtained using the Kissinger equation ($n = m = 1$).

4. During cooling of the melt with the highest TiO_2 and ZrO_2 concentrations, exothermic effects associated with baddeleyite and zirconolite crystallization are detected. Baddeleyite nucleates heterogeneously for low undercooling giving large crystals. For higher undercooling, zirconolite nucleates heterogeneously and grows on baddeleyite crystals.

References

1. A. E. RINGWOOD, S. E. KESSON, K. D. REEVE, D. M. LEVINS and E. J. RAMM, in "Radioactive Waste Forms for the Future," edited by W. Lutze and R. C. Ewing (Elsevier, Amsterdam, 1988) p. 233.
2. H. J. ROSSELL, *J. Solid State Chem.* **99** (1992) 38.
3. R. GIERE, C. T. WILLIAMS and G. R. LUMPKIN, *Schweiz. Mineral. Petrogr. Mitt.* **78** (1998) 433.
4. P. LOISEAU, D. CAURANT, O. MAJERUS, N. BAFFIER and C. FILLET, *J. Mater. Sci.* **38** (2003).
5. K. MATUSITA and S. SAKKA, *Bull. Inst. Chem. Res., Kyoto Univ*. **59**(3) (1981) 159.
6. *Idem., J. Non-Cryst. Solids* **38/39** (1980) 741.
7. D. R. MACFARLANE, M. MATECKI and M. POULAIN, *ibid.* **64** (1984) 351.
8. K. MATUSITA, K. MIURA and T. KOMATSU, *Thermochimica Acta* **88** (1985) 283.
9. C. S. RAY, Q. YANG, W.-H. HUANG and D. E. DAY, *J. Amer. Ceram. Soc*. **79**(12) (1996) 3155.
10. J. ROCHERULLE, *Mat. Res. Bull.* **35** (2000) 2353.
11. A. MAROTTA and A. BURI, *Thermochimica Acta* **25** (1978) 155.
12. N. KOGA, J. SESTAK and Z. STRNAD, *ibid.* **203** (1992) 361.
13. X. J. XU, C. S. RAY and D. E. DAY, *J. Amer. Ceram. Soc.* **74**(5) (1991) 909.
14. A. MAROTTA, A. BURI and F. BRANDA, *J. Mater. Sci*. **16** (1981) 341.
15. W. LI and B. S. MITCHELL, *J. Non-Cryst. Solids* **255** (1999) 199.
16. J. A. AUGIS and J. E. BENNET, *J. Thermal Analysis* **13** (1978) 283.
17. R. C. DEVRIES, R. ROY and E. FR. OSBORN, *J. Amer. Ceram. Soc.* **38**(5) (1955) 161.
18. "Phase Diagrams for Ceramists" (Am. Ceram. Soc., 1964) p. 219.
19. G. W. SCHERER, in "Materials Science and Technology. Glass and Amorphous Materials," Vol. 9, edited by R. W. Cahn, P. Haasen and E. J. Kramer, vol. edited by J. Jarzycki (1991), p. 119.
20. D. R. UHLMANN, in "Nucleation and Crystallization in Glasses." "Advances in Ceramics" Vol. 4, edited by J. H. Simmons, D. R. Uhlmann and G. H. Beall (The Am. Ceram. Soc., 1982) p. 80.
21. P. J. HAYWARD, E. R. VANCE and D. C. DOERN, *Am. Ceram. Soc. Bull.* **66**(11) (1987) 1620.
22. E. R. VANCE, C. J. BALL, M. G. BLACFORD, D. J. CASSIDY and K. L. SMITH, *J. Nucl. Mater.* **175** (1990) 58.
23. W. J. WEBER, J. W. WALD and Hj. MATZKE, *ibid.* **138** (1986) 196.
24. C. R. LUMPKIN, R. C. EWING, B. C. CHAKOUMAKOS, R. B. GREEGOR, F. W. LYTLE, E. M. FOLTYN, F. W. CLINARD JR., L. A. BOATNER and M. M. ABRAHAM, *J. Mater. Res*. **1**(4) (1986) 564.
25. F. FARGES, R. C. EWING and G. E. BROWN JR, *ibid.* **8**(8) (1993) 1983.
26. B. M. GATEHOUSE, I. E. GREY, R. J. HILL and H. J. ROSSELL, *Acta Cryst.* B **37** (1981) 306.
27. F. FARGES, G. E. BROWN JR, A. NAVROTSKY, H. GAN and J. J. REHR, *Geochim. Cosmochim. Acta* **60**(16) (1996) 3039.
28. F. FARGES, C. W. PONADER and G. E. BROWN JR., *ibid.* **55** (1991) 1563.
29. L. GALOISY, E. PELEGRIN, M.-A. ARRIO, P. ILDEFONSE and G. CALAS, *J. Amer. Ceram. Soc.* **82**(8) (1999) 2219.
30. P. LOISEAU, Ph.D. thesis, Université Paris VI, France, 2001.
31. E. R. VANCE, D. J. CASSIDY, C. J. BALLAND and G. J. THOROGOOD, *J. Nucl. Mater.* **190** (1992) 295.
32. R. J. KIRKPATRICK, L. KLEIN, D. R. UHLMANN and J. H. HAYS, *J. Geophys. Res.* **84**(B7) (1979) 3671.
33. P. LOISEAU, D. CAURANT, L. MAZEROLLES, N. BAFFIER and C. FILLET, in Scientific Basis for Nuclear Waste Management XXIV, *Mat. Res. Soc. Symp. Proc.* **663** (2001) 179.
34. P. LOISEAU, D. CAURANT, N. BAFFIER and C. FILLET, *Verre* **7**(1) (2001) 8.

Received 9 August 2001
and accepted 24 September 2002